ISSN 1063-7826, Semiconductors, 2020, Vol. 54, No. 8, pp. 838–843. © Pleiades Publishing, Ltd., 2020.

SURFACES, INTERFACES, AND THIN FILMS

A Comparative Study on CdS Film Formation under Variable and Steady Bath-Temperature Conditions

R. K. K. G. R. G. Kumarasinghe[a,b], W. G. C. Kumarage[c], R. P. Wijesundera[d], N. Kaur[e], E. Comini[e], and B. S. Dassanayake[a,b,*]

[a] *Postgraduate Institute of Science, University of Peradeniya, Peradeniya, Sri Lanka*

[b] *Department of Physics, University of Peradeniya, Peradeniya, Sri Lanka*

[c] *Research and International Affairs, Sri Lanka Technological Campus, Padukka, Sri Lanka*

[d] *Department of Physics, Faculty of Science, University of Kelaniya, Kelaniya, Sri Lanka*

[e] *Department of Information Engineering, Universitá Degli Studi Di Brescia, Brescia, Italy*

**e-mail: buddhikad@pdn.ac.lk*

Received October 16, 2019; revised December 16, 2019; accepted February 18, 2020

Abstract—The deposition temperature of the bath in chemical-bath-deposited cadmium-sulfide thin films can directly affect the optical, electrical, structural as well as morphological properties of deposited thin films. The reporting work discusses the properties of chemical-bath-deposited cadmium-sulfide thin films deposited under steady chemical-bath temperature conditions at both 40 and 80°C and compares with films formed under variable bath-temperature conditions by varying the temperature of the chemical bath from 40 to 80°C and 80 to 40°C while depositing. The optical, electrical, structural, and morphological properties of the deposited films were examined by using ultraviolet-visible spectroscopy, photo-electrochemical cell, Mott–Schottky measurements, grazing incident X-ray diffractograms, scanning electron microscopy, and profilometry. According to the results, films deposited under steady chemical-bath temperature conditions show better optoelectronic properties compared to the rest, while films fabricated at 40°C are the best.

Keywords: CBD, CdS, bath temperature, variable bath temperature, steady bath temperature

DOI: 10.1134/S1063782620080126

1. INTRODUCTION

Cadmium sulfide (CdS) has been identified as a popular candidate for applications such as large-area electronic devices and solar cells when considering the group II and VI semiconductor compounds [1]. CdS is also considered as a good partner to be used as the window layer material for cadmium telluride (CdTe) based solar cells due to low resistivity [2], high transparency [3], better interconnectivity [4], and roughness [5].

Chemical-bath deposition (CBD) is a process which is used to produce high quality CdS thin films at various temperature conditions and it is a popular deposition technique compared to the other deposition methods of CdS because of its advantages such as its simplicity, ability to large-area deposition and low cost of production, better adherence and reproducibility [6, 7]. The bath temperature of the CBD CdS is a conclusive factor which can affect optical, electrical, morphological and structural properties of deposited thin films [8].

In CBD, solid material is formed after the solution bath is supersaturated. There are two prominent reactions of forming solid materials called; homogeneous (within the bulk of the solution) and heterogeneous (at a surface, the substrate or random reaction on the reaction vessel surface) precipitation. The heterogeneous reaction has the tendency of film formation. When considering the formation of thin films, there are two main possible mechanisms or models; (a) ion by ion mechanism where the ions condense at the reacting surface to form film and (b) cluster by cluster mechanism where agglomeration of colloidal particles pre-formed in solution leads by absorption at the surface to form films [9].

The reporting work focuses on deposition and characterization of CBD-CdS thin films grown under stable bath-temperature conditions at 40 and 80°C (where ion-by-ion and cluster-by-cluster mechanisms take place, respectively) and under variable bath conditions by varying the deposition bath temperature from 40 to 80°C and 80 to 40°C. The optical, electrical, structural, and morphological properties of the fabricated films have been examined by using UV–Vis spectroscopy, photo-electrochemical (PEC) cell, $1/C^2$ vs. V measurements, grazing incident X-ray diffrac-

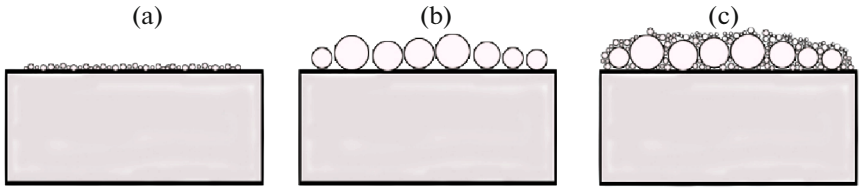

Fig. 1. An illustration of the processes that lead to thin film formation: (a) ion-by-ion; (b) cluster-by-cluster; (c) ion-by-ion infilling on cluster-by-cluster CdS.

tometer (GIXRD), scanning electron microscopy (SEM), and profilometry.

2. EXPERIMENTAL DETAILS

2.1. Growth Kinetics

Formation of CdS thin films at lower temperatures through ion-by-ion mechanism occurs by sequential ionic reactions. The basis of this mechanism is given by

$$Cd^{2+} + S^{2-} \rightarrow CdS. \quad \text{(i)}$$

If the ion product $[Cd^{2+}][S^{2-}]$ exceeds the solubility product (K_{sp}) of CdS then, neglecting kinetic problems of nucleation, CdS will form as a solid phase.

During this process, the presence of a surface (substrate or the walls of the reaction vessel) introduces a degree of heterogeneity that facilitates nucleation. Hence, the ion-by-ion depositions are more likely to take place on the substrate or the other surfaces. Here, the surface can be considered to be a catalyst for the nucleation process [10].

In the cluster-by-cluster process, agglomeration of colloidal cadmium hydroxide ($Cd(OH)_2$) particles that are pre-formed in solution through homogeneous nucleation gets adsorbed to the substrate surface to form a solid thin film through the following reactions:

$$Cd^{2+} + 2OH^- \leftrightarrow Cd(OH)_2\downarrow, \quad \text{(ii)}$$

$$nCd(OH)_2 + nS^{-2} \leftrightarrow (CdS)n\downarrow + H_2O, \quad \text{(iii)}$$

$$Cd(OH)_2 + 4NH_2OH \leftrightarrow [Cd(NH_3)_4]_2 + H_2O. \quad \text{(iv)}$$

Finally, the sulfide ions and $[Cd(NH_3)_4]^{2+}$ react to form CdS as mentioned below:

$$[Cd(NH_3)_4]n^{2+} + S^{2-} \leftrightarrow (CdS)n\downarrow + 4NH_3. \quad \text{(v)}$$

As indicated in reaction (iv), the metathetical reaction between the surface-bound "$Cd(OH)_2$ nuclei" and sulfide ions or thiourea through a heterogeneous process forms good-quality CdS thin films. Those adherent thin films are only obtained from baths which are supersaturated with respect to the precipitation of cadmium hydroxyl species, irrespective of the substrate used [11].

Considering the mechanism of film formation, it is expected that films produced through ion-by-ion deposition tend to produce smoother films compared to films that underwent cluster-by-cluster mechanism as shown in Figs. 1a and 1b [12]. Therefore, it can be hypothesized in the sample grown under variable bath temperature from 80 to 40°C, that a CdS layer may deposit through ion-by-ion mechanism on top of another CdS layer deposited through cluster-by-cluster mechanism and would generate a dense CdS film with a smooth surface as shown in Fig. 1c, due to ion-by-ion infilling on clusters. Contrariwise, cluster-by-cluster layer deposition of CdS on top of ion-by-ion CdS layer can produce rough surfaces compared to the previous, in which ion-by-ion layer would act as a seed layer for cluster-by-cluster deposited CdS thin film [9].

3. METHODOLOGY

CdS thin films were deposited onto fluorine-doped tin oxide (FTO, ~10 Ω/□, TEC 10, Sigma-Aldrich, USA) conducting glass substrates by CBD method at different bath temperatures. The solution was prepared in a ~250-mL container by adding 10 mL of 0.001 M cadmium sulfate ($CdSO_4$, 99%, Sigma-Aldrich), 1.1 mL of ammonia solution (NH_3, 35 wt %, Surechem) and deionized water to make the final volume 140 mL while 10 mL of 0.002 M thiourea ($CS(NH_2)_2$), 99%, Sigma-Aldrich) was added drop by drop into the bath throughout the experiment. Glass substrates were cleaned by using the standard procedure [13, 14] and positioned inside a bath at an angle of 45° using a Teflon sample holder for the CBD-CdS process. The bath was maintained under constant stirring during the deposition and the temperatures were kept constant for the films deposited under steady bath temperature conditions at 80°C (S_{80}) and 40°C (S_{40}), while the bath temperature was varied from 40 to 80°C and 80 to 40°C for the samples deposited under variable bath-temperature conditions ($S_{40–80}$ and $S_{80–40}$, respectively) for one hour. All the samples were deposited so that the film thicknesses were almost similar (~80 nm). After deposition, the CdS films were washed ultrasonically to remove the loosely attached CdS particles on the film. Then, CdS was removed from the non-conducting side of the substrate by chemical etching using diluted HCl. After washing the films with de-ionized water, they were dried with N_2

gas and finally annealed at 200°C for one hour in a vacuum furnace (Gallenkamp).

4. CHARACTERIZATION

Structural analysis of the grown thin films was conducted using PANalytical diffractometer (Empyrean) GIXRD using CuK_α radiation with $\lambda = 1.54184$ Å, glancing incident angle of 2° in continuous mode at generator voltage of 40 kV in 40-mA tube current using 0.05° scan step size with step time 2 s and 2θ in the range of 20°–70°. Thickness measurements of the thin films were made using an XP-1 Profilometer (AmbiosTechnology). A UV-1800 Shimadzu double-beam UV–Vis spectrophotometer was used for optical transmittance and absorbance measurements at room temperature under normal incidence in the wavelength range from 300 to 800 nm. Imaging of the microstructure was done using Zeiss EVO/LS15 scanning electron microscope. The $I(V)$ (current vs. voltage) measurements were obtained in a PEC Cell-L01 containing 0.1 M of $Na_2S_2O_3$ (97%, Baxter Smith Labs, USA) keeping the area of the CdS/electrolyte was 0.25 cm^2. The junction was illuminated under an AM 1.5 simulated solar light irradiation using a 150 W short-arc xenon lamp. The $1/C^2$ vs. V measurements were carried out in the same PEC cell within the potential range from +0.8 to –0.8 V, scanning in the cathodic direction using Gamry (G300) potentiostat. The solid|liquid junction was held at 0.2 V and 1000 Hz with respect to the Ag/AgCl reference electrode during the Mott–Schottky measurements. For I–V and Mott–Schottky measurements, Pt and Ag/AgCl electrodes were used as counter and reference electrodes, respectively.

5. RESULTS AND DISCUSSION

5.1. GIXRD Results

The GIXRD diffractograms of samples S_{40}, $S_{40–80}$, $S_{80–40}$, S_{80}, bare FTO, and CdS on borosilicate glass are shown in Fig. 2. All films were hexagonal with a main (002) reflection and weaker (100), (101), (110), and (103) planes of CdS (JCPDS 80-0006), to account for the crystalline structure of CdS thin films deposited. Further, the peaks other than explained above are related to the FTO glass substrate which can be confirmed by diffractrogram of bare FTO in Fig. 2e. CdS deposited on borosilicate glass substrate shown in Fig. 2f also confirms that the films are primarily hexagonally oriented.

The texture coefficient (TC_{hkl}) [15–18] can be used to describe the preferential orientation of the crystallites along a crystal plane (*hkl*) in a thin film and it is determined from the GIXRD spectra of the CdS films

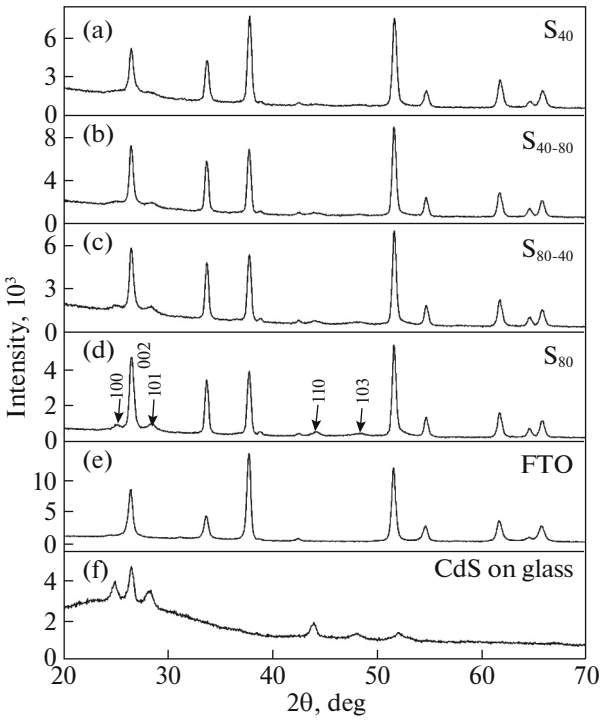

Fig. 2. GIXRD difrractograms of (a) S_{40}, (b) $S_{40–80}$, (c) $S_{80–40}$, (d) S_{80}, (e) bare FTO, and (f) CdS on borosilicate glass.

S_{40}, $S_{40–80}$, $S_{80–40}$, and S_{80}, according to the formula [19–21];

$$TC_{hkl} = \frac{I_{(hkl)}/I_{0(hkl)}}{1/n\sum_{h'k'l'} I_{(h'k'l')}/I_{0(h'k'l')}}, \quad (1)$$

where $I_{(hkl)}$ is the measured relative intensity of plane (*hkl*), $I_{0(hkl)}$ is the standard intensity of the plane (*hkl*) taken from JCPDS data (JCPDS 06-0314), and n is the number of diffraction peaks that is equal to 5 in this work, with most intense reflections (002), (100), (101), (110), and (103). For a preferential orientation, TC_{hkl} should be greater than one. According to the results, (002) appears to be the most preferred orientation for all fabricated samples.

5.2. Optical Measurements

UV–Vis spectroscopy was used to measure the transmittance and the absorption of deposited films. Figure 3 shows the optical transmittance spectra of the deposited CdS samples.

According to the UV–Vis spectroscopic results, S_{40} has highest transmittance while the lowest transmittance is recorded for S_{80}. Additionally, according to Fig. 3, there is a clear red shift of the transmittance edge of the sample S_{80} and $S_{80–40}$ compared to the

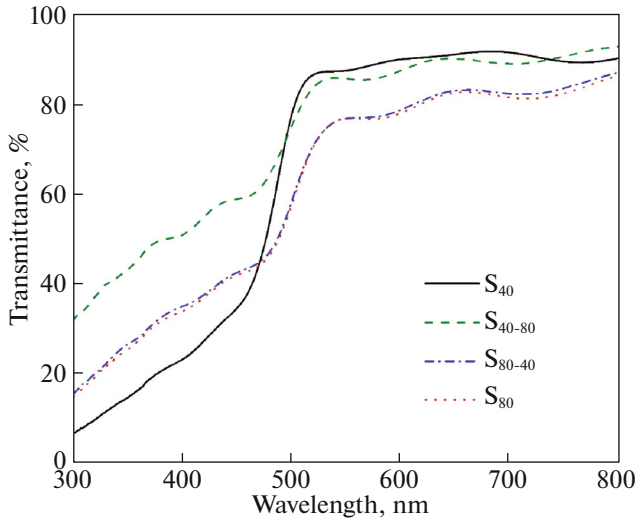

Fig. 3. The optical transmittance of samples S_{40}, $S_{40–80}$, $S_{80–40}$, and S_{80}.

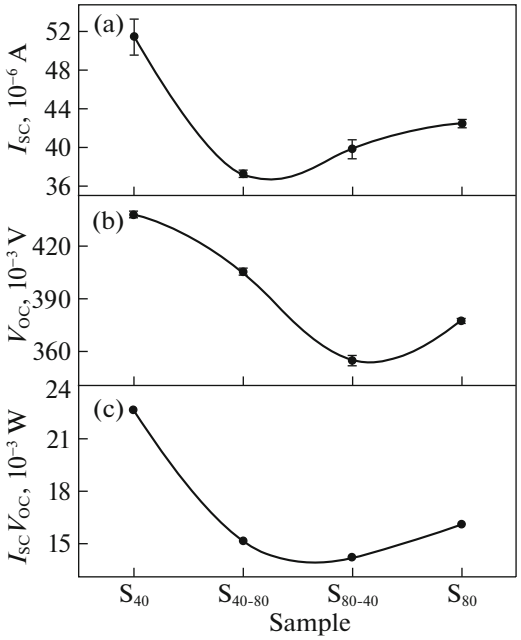

Fig. 4. Variation of (a) I_{SC}, (b) V_{OC}, and (c) $I_{SC} \cdot V_{OC}$ of CBD–CdS samples.

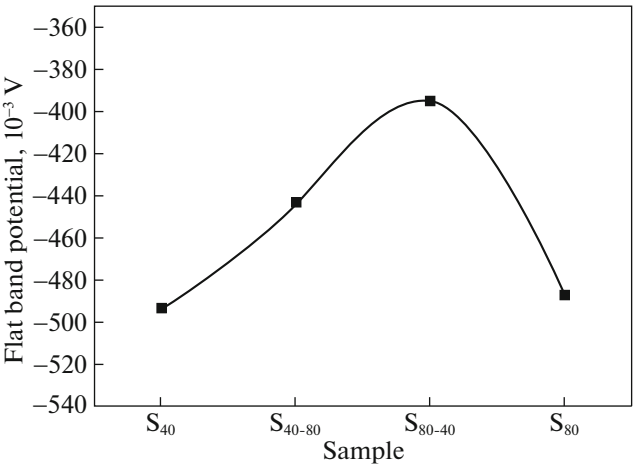

Fig. 5. Variation of flat-band potential of samples S_{40}, $S_{40–80}$, $S_{80–40}$, and S_{80}.

other two, suggesting that the band gaps of the deposited films are subjected to alternation.

The band gap (E_g) values of the deposited samples were estimated using the Beer–Lambert's law which shows in the equations below,

$$\alpha d = \ln\left(\frac{I_0}{I_T}\right)^{1/2} = 2.303Abs, \quad (2)$$

$$\alpha h\nu = A(h\nu - E_g)^{1/2}, \quad (3)$$

where d is the film thickness, I_0 is the incident intensity, I_T is the transmittance intensity, Abs is the absorbance, α is the absorption coefficient of the film, A is a material-dependent constant, h is Planck's constant, E_g is the band gap, and v is the frequency of the light. The band-gap values of CdS thin films were obtained by extrapolating the linear $(\alpha h\nu)^2$ vs. $h\nu$ plots derived from the Eq. (3), to $(\alpha h\nu)^2 = 0$ [22]. The calculated E_g shows that the sample S_{40} has the highest E_g, while other samples are not found to show any significant variation. Since the optical properties and electrical properties of the films are correlated, the electrical properties of the films were studied via PEC and Mott–Schottky measurements.

5.3. Electrical Measurements

The electrical measurements of the deposited samples are shown in Fig. 4. According to Fig. 4, the highest short-circuit current (I_{SC}), open-circuit voltage (V_{OC}) as well as $I_{SC} \cdot V_{OC}$ was obtained for the sample S_{40}. The variation of V_{OC} with respect to the deposited different samples was also found to agree with the variation of band gap.

The flat-band potential (V_{fb}) and carrier concentration (N_D) were calculated from the X-axis intercept and the slope of the line fits of the Mott–Schottky equation [23, 24];

$$\frac{1}{C^2} = \frac{2}{\varepsilon\varepsilon_0 A N_D}\left(V - V_{fb} - \frac{kT}{e}\right),$$

where e is the electron charge, ε (= 8.5) is the dielectric constant, ε_0 is the permittivity in vacuum [25]. The Mott–Schottky plots (not shown) confirmed the n-type behavior of all the fabricated CdS thin films. The highest flat-band potential value was recorded for the

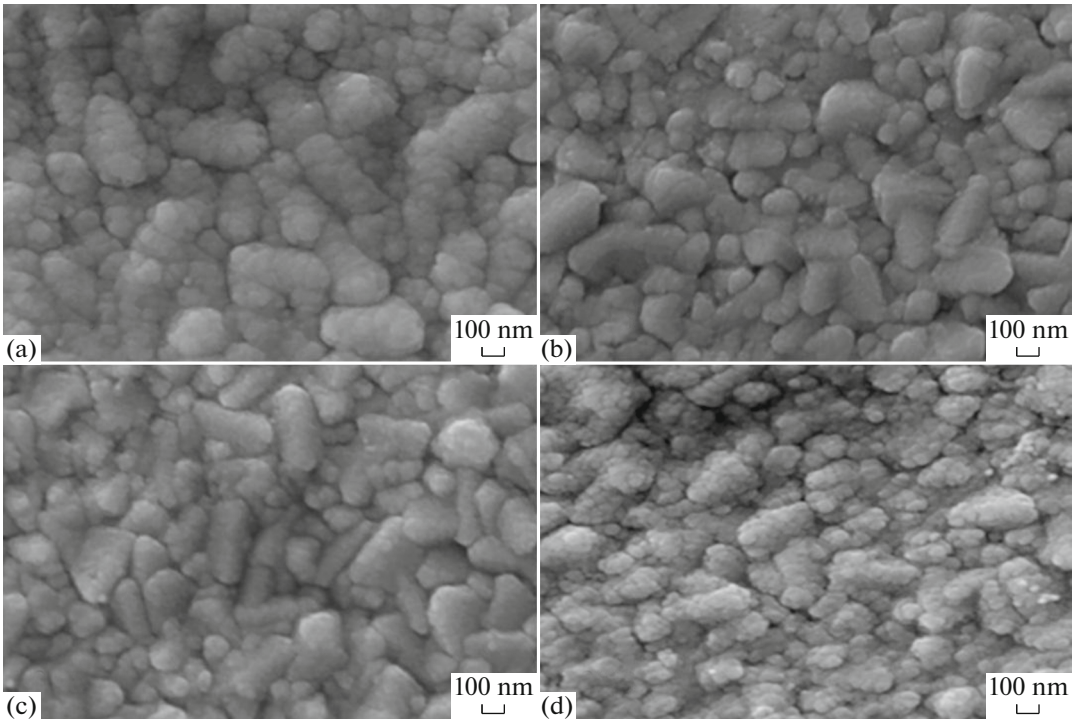

Fig. 6. SEM micrograms of the fabricated CdS samples: (a) S_{40}, (b) $S_{40–80}$, (c) $S_{80–40}$, (d) S_{80}.

thin film deposited at 40°C (Fig. 5). Higher V_{fb} yields higher electric field strength in the space-charge region of the semiconductor, enhancing the V_{OC} value. Therefore, the similar trends in the variation of both V_{OC} and the V_{fb} in Fig. 4b and Fig. 5 might be due to this effect.

Furthermore, one potential reason for the highest I_{SC} value observed in Fig. 4 for the thin film deposited at 40°C (S_{40}) can also be due to the high flat-band potential [26]. When the carrier concentration values were calculated using the above equation, it was found that all the carrier concentrations were in the order of 10^{16} cm^{-3}, while samples $S_{40–80}$ and $S_{80–40}$ showed higher values compared to the rest.

5.3. Morphological Results

Figures 6a–6d shows SEM micrographs for four CdS thin films grown at different bath conditions.

According to the SEM images, both the samples S_{40} and S_{80} share a common feature, where smaller clusters seems to be distributed on top of large clusters, unlike in the case of samples $S_{80–40}$ and $S_{40–80}$. This feature can increase the effective surface area of the samples S_{40} and S_{80} compared to the rest. In addition, it is also evident from the SEM images that the sample S_{40} seems to have better interconnectivity compared to sample S_{80}. Therefore, it is possible to further justify the higher I_{SC} value obtained for S_{40} compared to the rest of the samples. Also, when comparing $S_{80–40}$ and $S_{40–80}$, $S_{80–40}$ shows better interconnectivity than the $S_{40–80}$, which can be seen in Fig. 6. This effect can be due to the ion-by-ion infilling on the cluster-by-cluster CdS. Therefore, the I_{SC} value of $S_{80–40}$ is expected to be comparably higher than $S_{40–80}$. Furthermore, as seen by SEM images in Fig. 6d, film surface of S_{80} has rougher topography compared to S_{40}. Rough surfaces tend to scatter much light and hence give a way to low transmittance [27]. Hence this could be the reason for the higher transmittance recorded for S_{40}, as seen in Fig. 3.

6. CONCLUSIONS

Cadmium-sulfide (CdS) thin films were successfully deposited by the chemical-bath deposition (CBD) method under stable bath-temperature conditions at 40 and 80°C and under variable bath conditions by varying the bath temperature from 40–80°C and 80–40°C while depositing. GIXRD analysis indicates the formation of hexagonal phase of CdS with (002) preferred orientation for films deposited under both constant and variable temperature conditions while the sample deposited at 80°C showed better crystallinity. Moreover, SEM investigations suggest an infilling of CdS in sample $S_{80–40}$ when bath temperature is lowered from an initial high temperature. Resulting lower surface roughness of $S_{80–40}$ suggests lower effective surface area, which in turn facilitates

low I–V values. According to the optical, morphological, and electrical results, even though small clusters formed due to ion-by-ion deposition may have acted as seeds for cluster-by-cluster deposition of CdS in S_{40-80}, films deposited at 40°C display better electrical as well as optical properties owing primarily to morphological properties.

ACKNOWLEDGMENTS

Professor S. Sivananthanthan of the University of Illinois, Chicago, USA, Professor M.A.K.L. Dissanayake of the National Institute of Fundamental Studies (NIFS), Sri Lanka, and Mr. A.G.A.B. Dissanayake of Postgraduate Institute of Science, University of Peradeniya, Sri Lanka are acknowledged for their valuable suggestions and support. Part of the research was performed at the Sensor Lab, Department of Information Engineering, Universitá Degli Studi Di Brescia, Brescia, Italy.

CONFLICT OF INTEREST

The authors declare no conflict of interest.

REFERENCES

1. Z. Wei, Y. Wang, L. Ma, and X. S. Wu, Phys. B (Amsterdam, Neth.) **525**, 98 (2017).
2. R. Mendoza-Pérez, G. Santana-Rodríguez, J. Sastre-Hernández, A. Morales-Acevedo, A. Arias-Carbajal, O. Vigil-Galan, J. C. Alonso, and G. Contreras-Puente, Thin Solid Films **480–481**, 173 (2005).
3. A. M. Acevedo, Sol. Energy Mater. Sol. Cells **90**, 2213 (2006).
4. N. R. Paudel, C. Xiao, and Y. Yan, J. Mater. Sci. Mater. Electron. **25**, 1991 (2014).
5. H. Moualkia, S. Hariech, and M. S. Aida, Mater. Sci. Forum **609**, 243 (2009).
6. F. Liu, Y. Lai, J. Liu, B. Wang, S. Kuang, Z. Zhang, J. Li, and Y. Liu, J. Alloys Compd. **493**, 305 (2010).
7. L. E. Trujillo, E. A. Chávez-Urbiola, F. Legorreta, I. R. Chávez-Urbiola, F. J. Willars-Rodriguez, R. Ramírez-Bon, and M. Ramárez-Cardona, J. Cryst. Growth. **478**, 140 (2017).
8. S. M. Kwon, S. M. Kim, and C. W. Jeon, Curr. Appl. Phys. **17**, 92 (2017).
9. P. O'Brien and J. McAleese, J. Mater. Chem. **8**, 2309 (1998).
10. G. Hodes, *Chemical Solution Deposition of Semiconductor Films* (Marcel Dekker, New York, 2002).
11. S. Prabahar and M. Dhanam, J. Cryst. Growth **285**, 41 (2005).
12. W. G. C. Kumarage, R. P. Wijesundera, V. A. Seneviratne, C. P. Jayalath, and B. S. Dassanayake, J. Phys. D: Appl. Phys. **49**, 095109 (2016).
13. P. K. K. Kumarasinghe, A. Dissanayake, B. M. K. Pemasiri, and B. S. Dassanayake, Mater. Res. Bull. **96**, 188 (2017).
14. W. G. C. Kumarage, R. P. Wijesundera, V. A. Seneviratne, C. P. Jayalath, T. Varga, M. I. Nandasiri, and B. S. Dassanayake, Mater. Chem. Phys. **200**, 1 (2017).
15. P. K. K. Kumarasinghe, A. Dissanayake, B. M. K. Pemasiri, and B. S. Dassanayake, J. Mater. Sci.: Mater. Electron. **28**, 276 (2017).
16. G. Zoppi, K. Durose, S. J. C. Irvine, and V. Barrioz, Semicond. Sci. Technol. **21**, 763 (2006).
17. S. Gupta and K. Munirathnam, Indian J. Pure Appl. Phys. **52**, 44 (2014).
18. P. K. K. Kumarasinghe, A. Dissanayake, B. M. K. Pemasiri, and B. S. Dassanayake, Mater. Sci. Semicond. Process. **58**, 51 (2017).
19. V. Bilgin, S. Kose, F. Atay, and I. Akyuz, J. Mater. Sci. **40**, 1909 (2005).
20. R. Mariappan, M. Ragavendar, and V. Ponnuswamy, J. Alloys Compd. **509**, 7337 (2011).
21. S. Du and Y. Li, Adv. Mater. Sci. Eng. **2015**, 969580 (2015).
22. H. Moualkia, G. Rekhila, M. Izerrouken, A. Mahdjoub, and M. Trari, Mater. Sci. Semicond. Process. **21**, 186 (2014).
23. W. G. C. Kumarage, R. P. Wijesundera, V. A. Seneviratne, C. P. Jayalath, T. Varga, and B. S. Dassanayake, Appl. Phys. A **367**, 171 (2018).
24. S. R. Morrison, *Electrochemistry at Semiconductor and Oxidized Metal Electrodes* (Springer, New York, 1980).
25. M. E. Ozsan, D. R. Johnson, M. Sadeghi, D. Sivapathasundaram, G. Goodlet, M. J. Furlong, L. M. Peter, and A. A. Shingleton, J. Mater. Sci., Mater. Electron. **7**, 119 (1996).
26. M. Kostoglou, N. Andritsos, and A. J. Karabelas, Thin Solid Films **387**, 115 (2001).
27. F. Liu, Y. Lai, J. Liu, B. Wang, S. Kuang, Z. Zhang, J. Li, and Y. Liu, J. Alloys Compd. **493**, 305 (2010).